15-15Ti(Si) austenitic steel: creep behaviour in hostile environment

Alessandra Strafella, Antonino Coglitore, Paride Fabbri, Elena Salernitano
ENEA- Italian National Agency for New Technologies, Energy and Sustainable Economic Development-Laboratory of Materials Technologies Faenza, Via Ravegnana, 186 - 48018 - Faenza, Italy
alessandra.strafella@enea.it, antonino.coglitore@enea.it, paride.fabbri@enea.it, elena.salernitano@enea.it

ABSTRACT. This work aims at studying the creep behaviour of 15-15Ti(Si) austenitic steel, under uniaxial stress (range of 300-560 MPa), and its interaction with liquid lead. The steel was tested to verify its sensitivity to Liquid Metal Embrittlement (LME) and to simulate its behaviour in operating thermal and mechanical stress conditions of the IV generation Lead-cooled fast reactor. The experimental results permitted to plot the time-strain creep curve and the characteristic Norton-based curve, simulating the creep behaviour at all stress values. The comparison between the creep curves in air and in lead showed that the LME produces a decrease of creep-rupture time, a reduction of creep strain and then the loss of steel ductility. Moreover, the raw material and fracture surfaces were analyzed by Optical Microscope and Scanning Electron Microscope (SEM). SEM micrographs highlighted that lead changes both the mode and the type of specimen fracture. In addition, it was analyzed the lead action time, as the time after which the corrosion appears with macroscopic effects. Although some tests are still ongoing, it can be assumed that at high stresses, LME takes place after a long time of steel/lead contact while at low stresses, LME tends to prevail on creep effect.

KEYWORDS. 15-15Ti(Si); Austenitic stainless steel creep; Creep curves; Steady Strain Creep Rate; Liquid Metal Embrittlement (LME); Creep tests in lead.

Citation: Strafella, A., Coglitore, A., Fabbri, P., Salernitano, E., Frattura ed Integrità Strutturale, 42 (2017) 352-365.

Received: 08.08.2017
Accepted: 12.09.2017
Published: 01.10.2017

INTRODUCTION

Since several years, austenitic stainless steels are object of a great interest for their properties and then their applications in nuclear field. Creep strength and resistance to irradiation-induced void swelling are the main requirements for high temperature components of fast reactors. For these reasons, type 15-15Ti(Si) material which is a Ti-stabilized austenitic stainless-steel alloy, is one of most suitable for nuclear industry [1-3].
15-15Ti(Si) was designed around the standard AISI 316 stainless steel with a specifically tailored composition, especially regarding the carbon and titanium content, in order to limit irradiation induced void swelling [1].
The French work on irradiation of Rapsodie–Fortissimo demonstration reactor demonstrated that addition of titanium led to improved void swelling resistance of austenitic steel. Accordingly, the 15 Ni-15 Cr-Ti (named AIM1 or 15-15 Ti steel)

was developed and utilized in the PHÉNIX reactor where it exceeded the target burnup of 100 dpa. Addition of silicon to 15-15Ti further improved the swelling resistance. With silicon-modified 15-15Ti, the maximum fuel pin deformation was reduced by a factor of 2.4 as compared to the silicon-free 15-15Ti grade [3].
The addition of Ti also improves the high temperature mechanical properties due to the precipitation of carbide particles, either $M_{23}C_6$, or TiC in relation to the contents of Ni and Cr and to the matrix structure, grain size and dislocation density. It has been noticed for a long time that the high dislocation density found in cold-worked steels reduces the swelling. For this reason, Ti-modified austenitic stainless steels are often cold-worked to increase their mechanical properties. Dislocations trap vacancies and decrease their supersaturation. Nevertheless, a recovering of the dislocation network is observed at high temperature (T > 540 °C) and reactivates the swelling. Titanium has been added in the alloys to avoid this phenomenon. It induces the precipitation of nanosized titanium carbides which pin the dislocation network and stabilize it at high temperature. Indeed, the cold-working promotes the precipitation of carbides which are liable to precipitate on slip planes produced by pre-strain and creep strain. Therefore, the cold-worked steels have higher crack growth resistance at high stress intensity levels compared to solution-annealed stainless steel [4-7].
For its properties, 15-15Ti(Si) is one of the best candidates for high temperature components of nuclear reactor of IV generation Lead-cooled fast reactor (LFR) [2-3] which is one of the systems to be deployed in the future. The main problem in LFR reactor development is the compatibility of the structural materials (steels) with the coolant as well as the corrosion of structural components and fuel. When steel comes in contact with liquid metal, the loss of ductility in normally ductile steel could occur; this phenomenon is named Liquid Metal Embrittlement (LME) and takes place when steel is stressed in temperature under contact with liquid metal.
Although there is a great interest on these steel properties, only few data on its characterization can be found in the literature.
So, the aim of this work is the study of the 15-15Ti(Si) stainless steels creep properties both in air and in lead. For this purpose, the creep behaviour was investigated at 550° C, under a wide range of applied stresses, in hostile condition or in air , following by a morphological analysis of fracture surfaces.

EXPERIMENTAL PROCEDURE

Materials

Tests were carried out on creep specimens prepared from 15-15Ti(Si) steel, an austenitic steel provided by OCAS. The steel was manufactured in the form of plates (15mm X 750mm X 250mm), 20% cold-worked (CW): it was subjected to a homogenization annealing treatment in a furnace at 1230°C for 15h, hot-rolled at 1250°C for 1.5-2h, annealed at 1080°C (followed by a water-quench treatment) and 20% CW.
The steel was cold-worked because this process promotes the precipitation of carbides, which generally increases the mechanical properties of materials. Compared to solution-annealed stainless steel, the cold-worked steels have higher crack growth resistance at high stress intensity levels. The composition of 15-15Ti(Si) is given in Tab. 1.

All elements	C	Mn	Si	P	Ti	Cr	Ni	B	Mo
%	0.090	1.502	0.791	0.041	0.404	14.392	15.607	0.007	1.509

Table 1: Chemical composition of 15-15Ti(Si) steel

As anticipated in the previous paragraph, it must be underlined that the Ti presence in the steel is important for the purposes of this work because induces the precipitation of carbide particles, $M_{23}C_6$ or TiC, then improves the high temperature mechanical properties. Moreover, Ti addition decreases the irradiation swelling; that is important for nuclear applications.
The used lead is provided by Sigma-Aldrich in particles with a purity ≥ 99.9%, size ≤ 2 mm and melting point 327.4°C.

Specimens

Creep specimens were machined from the plate in the rolling direction to obtain 6 mm in diameter and 70 mm of gauge length, as shown in Fig. 1.

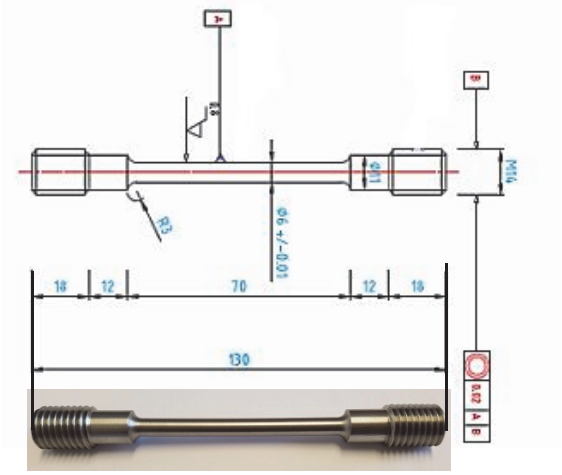

Figure 1: Creep specimen dimensions.

Creep tests

The creep tests were carried out in air and in stagnant lead, at 550°C that is typical working temperature of LFR. The loads were applied in uniaxial tensile mode; stress values were in the range of 300-560 MPa, which is lower than yield stress value (theoretical 620 MPa ≤ Rp0.002 ≤ 840 MPa, after 20% CW).

All tests were performed by MAYES machine with a maximum loading capacity of 20kN and maximum temperature of 1000°C. Because of the measurement uncertainty in the determination of the specimen cross section, the initial tensile stress was measured with an accuracy of ±3%. The specimen elongation during the tests was measured by monitoring in continuous the grip movement; Super Linear Variable Capacitor (SLVC) transducers were used for measuring and recording elongations smaller than 0.5 μm. The acquired data were plotted as conventional strain versus time curves. The matrix of main tests is shown in Tab. 2.

Material	Temp. [°C]	Stress [MPa]				
		300	400	500	560	575
15-15Ti(Si)	550°C	○	○	○, ●	○, ●	●

Table 2: Matrix of the main tests.

where "○" represents the creep test performed in air and "●" that in lead. A particular cell, showed in Fig. 2, was specifically designed and manufactured for tests in lead.

For the tests in lead, the creep machine is equipped with a specifically designed and manufactured cell, for the containment of the molten liquid metal, as shown in Fig. 2 and 3. The cell consists of a lead container to fully immerse the specimen during test, low and upper grips where the specimen is mounted to be subjected to tensile stress and rod grips for the SLVC to measure the sample elongation during the test. The whole testing cell apparatus is then put into the furnace.

The cell is mounted on a MAYES machine; specimen was fixed to the grips of cell, filled with solid lead, heated up to the lead melting temperature and then the test temperature and load were applied. Data points were acquired every 1 h.

Morphological and microstructural characterization

The steel, both raw and after rupture, was analyzed by Optical Microscope and Scanning Electron Microscope (SEM). The specimen surfaces were observed both before and after boiling glyceregia etching (30 mL HCI, 20 mL glycerol, 10 mL HNO_3). A Reichert-Jung MeF 3 optical microscope was used to observe the microstructure, while a SEM Leo 438 VP to characterize in high vacuum the morphology and microstructure of the specimens surfaces.

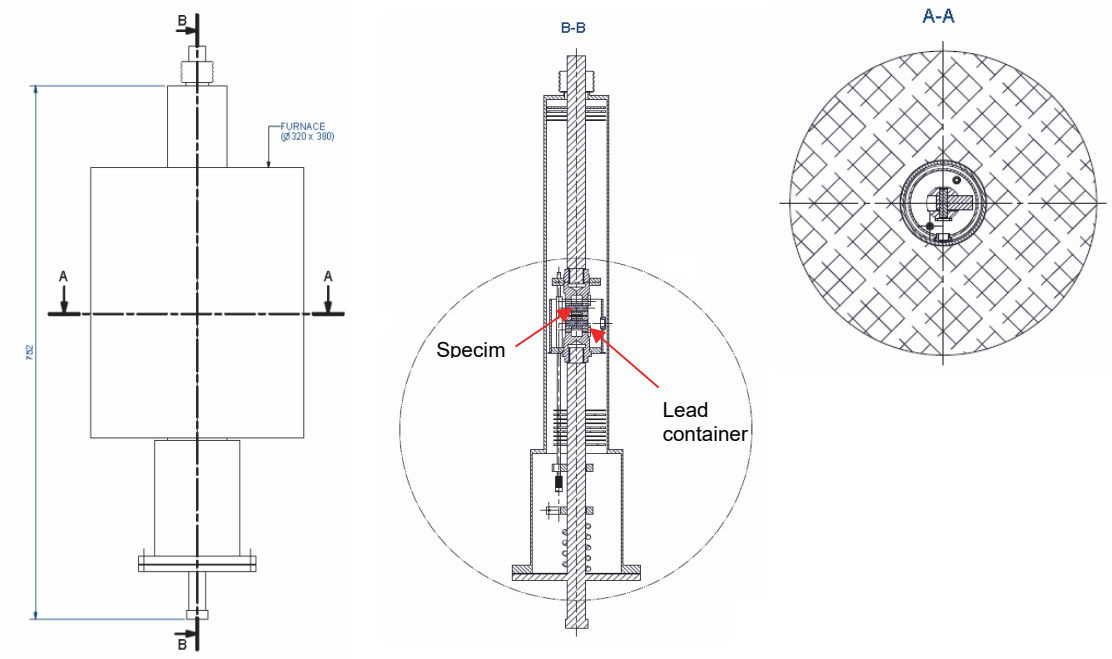

Figure 2: overall sketch of testing cell with both the longitudinal and cross sections.

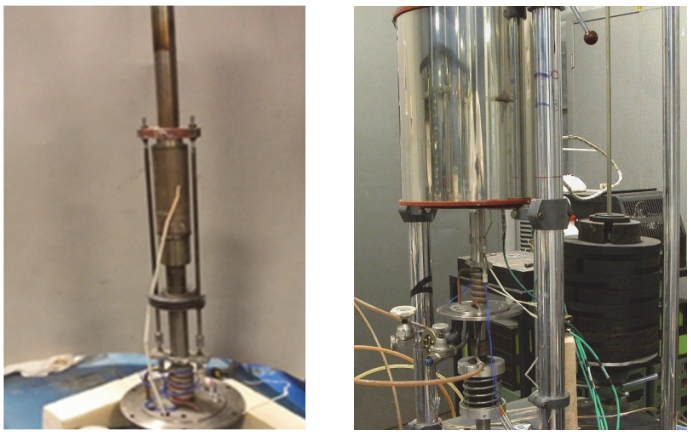

Figure 3: Cell assembly, designed and manufactured for tests in lead, on a MAYES machine during the specimen fixing and with its furnace.

RESULTS AND DISCUSSION

Creep curves in air

The specimens were tested at 550°C under constant loads, corresponding to the initial tensile stresses in the range of 300-560 MPa, and the experimental data allowed to obtain the typical creep curves of 15-15Ti(Si). The most relevant curves were depicted in Fig. 4, where the evolution of the creep strain with time at various stress levels is plotted.

If we consider the same time value in the graph, it can be observed that the creep strain increased with the applied stress; moreover it can also noticed that at 560MPa, the rupture was reached at 1165h, while the tests at 300, 400 and 500MPa are still in progress.

The shape of creep curve is consistent with the expectations: after long time (more than 1000h), at 300 and 400 MPa, the strain curves didn't reach the tertiary creep stage, still remaining in the secondary creep phase; at 500 MPa, although is still ongoing, the creep curve clearly shows a defined primary and secondary stages. At stress values near the yield strength of

15-15Ti, as 560MPa (theoretical 620MPa ≤ Rp0.002 ≤ 840MPa, after 20%CW), all the three phases of creep can be recognized.
These curves are plotted in Fig. 5 (until 1000h, current time value of test at 500MPa), providing important results on the creep behaviour because the secondary creep stage was reached and the duration was greater than of 1000h.

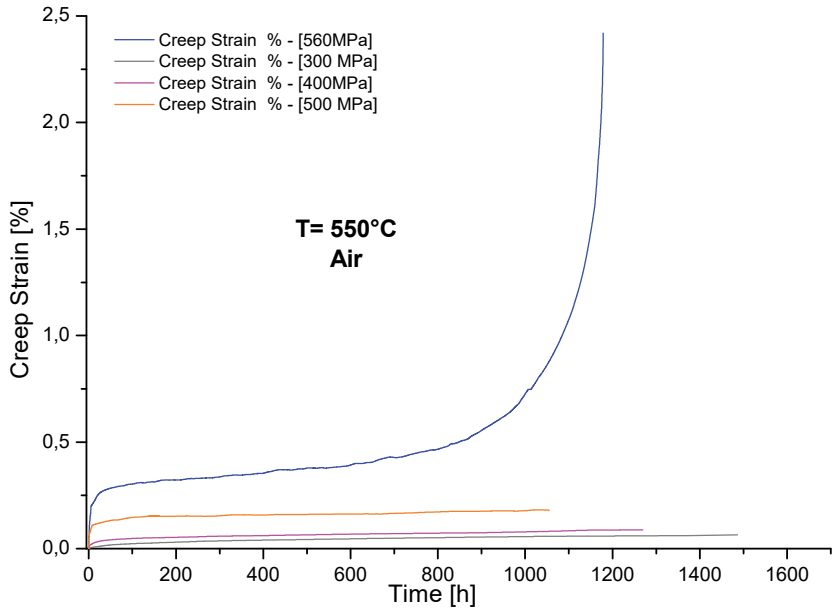

Figure 4: Comparison of 15-15Ti(Si) creep curves in air at 300, 400, 500 and 560 [MPa].

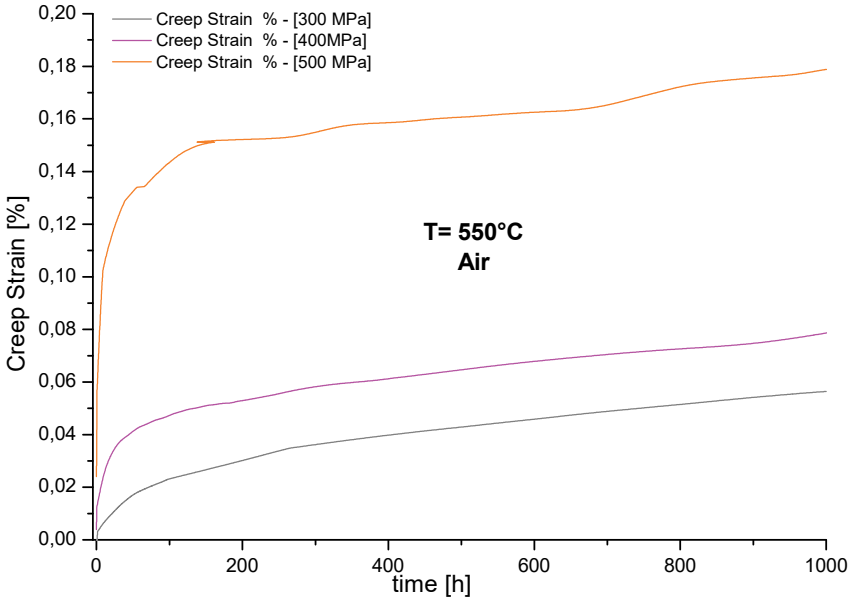

Figure 5: Comparison between creep curves in air at 300, 400 and 500 MPa, until 1000h.

All tests enabled to calculate the creep rate of secondary stage, also defined steady strain creep rate (sscr) being the minimum and constant creep rate.
The sscr values are obtained and compared with two methods, as illustrated in Fig. 6:

- Using the first derivative on curve strain-time to determinate the minimum;
- Plotting Fit linear of strain-time curve in secondary creep stage.

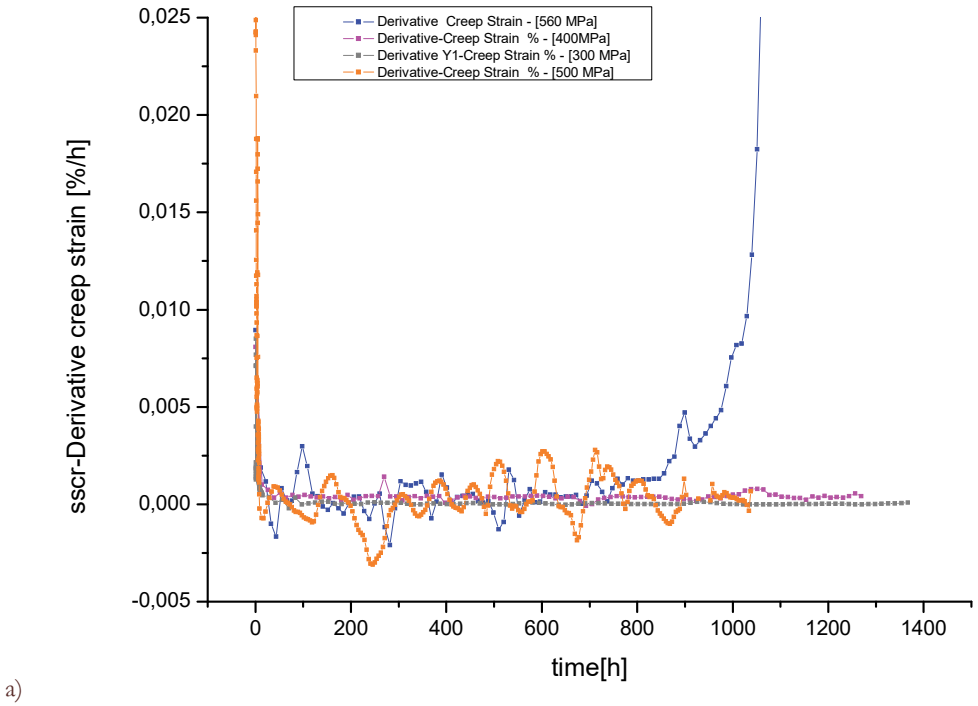

a)

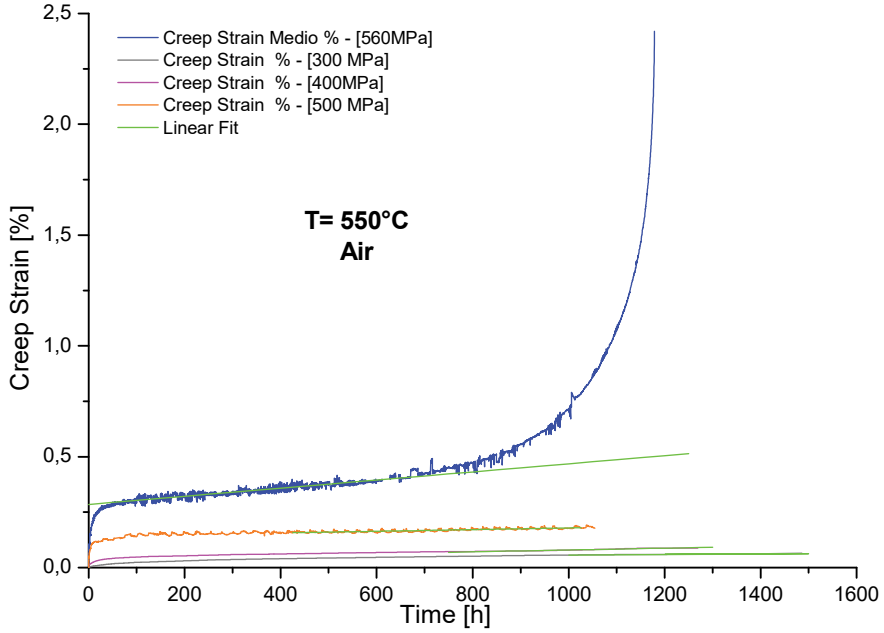

b)

Figure 6: sscr calculus: minimum of first derivative (a) and fit linear of secondary creep stage (b).

The steady strain creep rates were plotted in a log–log graph. Fig. 7 shows the variation of sscr with the applied stress. The variation of sscr with applied stress obeys a power law relationship in the form of Norton-type:

$$sscr = A\sigma^n \tag{1}$$

where σ is the applied stress, n is the stress exponent, and A is an empirical constant.
For 15-15Ti(Si) steel, the found A and n values are shown in Tab. 3.

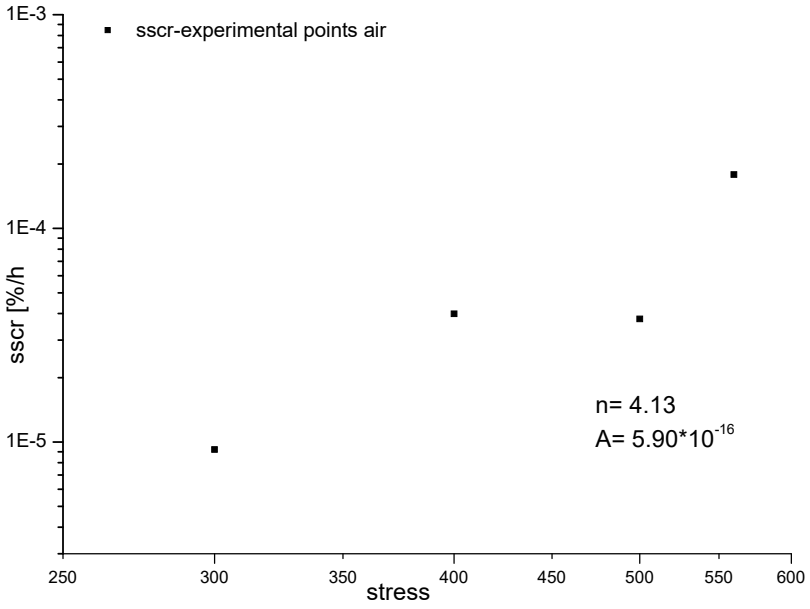

Figure 7: log–log plot of sscr-stress points.

A	n
$5.90*10^{-16}$	4.13

Table 3: Values of Norton-power law parameters.

The value of stress exponent **n** is indicative of the rate controlling deformation mechanism.
For austenitic stainless steels stress exponents are generally in the range of 3–12 and are associated with dislocation creep [10]. This is due to the nature of austenitic stainless steels which are solid solution alloys where the precipitation takes place during creep; for this reason, they show a particular behaviour which is intermediate between those of solid solution alloys and precipitation hardened/dispersion strengthened materials.
The literature data report a value of n=3–5 for pure metals and simple solid solution alloys where the main creep deformation mechanism is the dislocation creep; other major creep deformation mechanisms such as diffusion creep are characterized by n= 1, and grain boundary sliding controlled creep are identified with a value of n=2.
Instead, as also reported by literature, complex alloys and precipitation hardened/dispersion strengthened materials showed much higher values of n (≈40). It means that in austenitic stainless steels, the value of **n** is intermediate between those of solid solution alloys and precipitation hardened/dispersion strengthened materials and it is in a range of 3–12 [7].
The experimental analysis highlighted that the 15-15Ti(Si) austenitic steel value for the stress exponent is n=4.13; this result is consistent with the expectations and confirms that the steel deforms through the dislocation creep mechanism.
Based on the Norton power law, on experimental data and on calculated values of **n** and **A**, the characteristic creep curve sscr-stress (log–log plot) was plotted, enabling to simulate the creep behaviour in air at all stress values (Fig. 8).
These analyses could provide some important information for the use of this material in nuclear field because only few data can be found in the literature on 15-15Ti(Si) characterization.

Creep curves in lead

For its particular application on nuclear field, 15-15Ti(Si) was tested in lead in order to conduct a preliminary study on its lead corrosion sensitivity. A test at 575MPa and 550°C was performed to ascertain the correct working of new cell designed and manufactured for tests in liquid metal. The three stages are clearly recognized, as showed in Fig. 9.
The most important tests in lead were performed using the following parameters, deriving from tests in air:

- T= 550°C
- σ = 500 and 560 MPa

To date, the test at 500MPa is still in progress: the strain is 0.46% and the test duration is 885h. The comparison among all lead curves up to 600h is depicted in Fig. 10, where primary and secondary phases of creep are shown: it can be clearly recognized them and the calculation of sscr was possible.

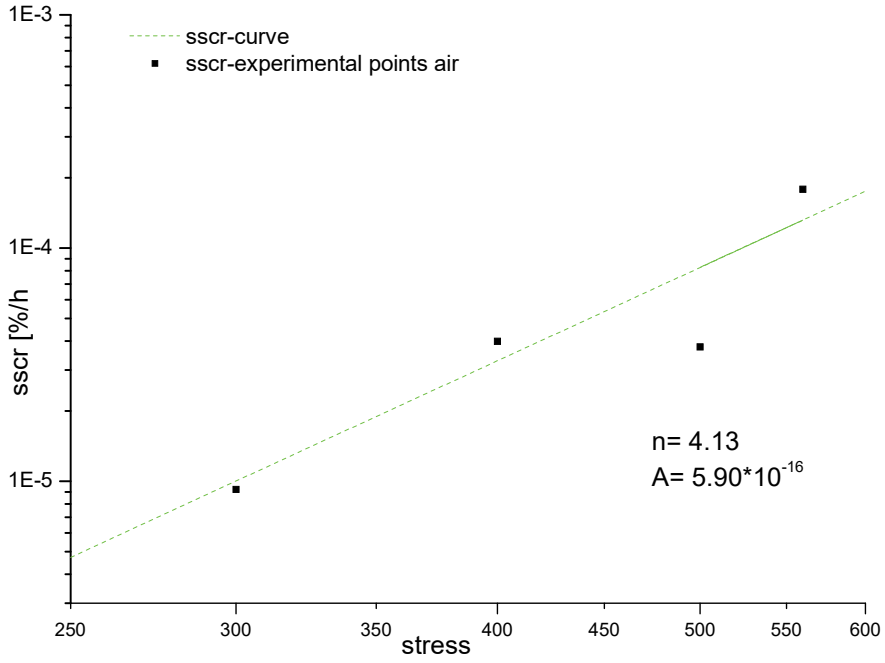

Figure 8: Characteristic creep curve sscr-stress.

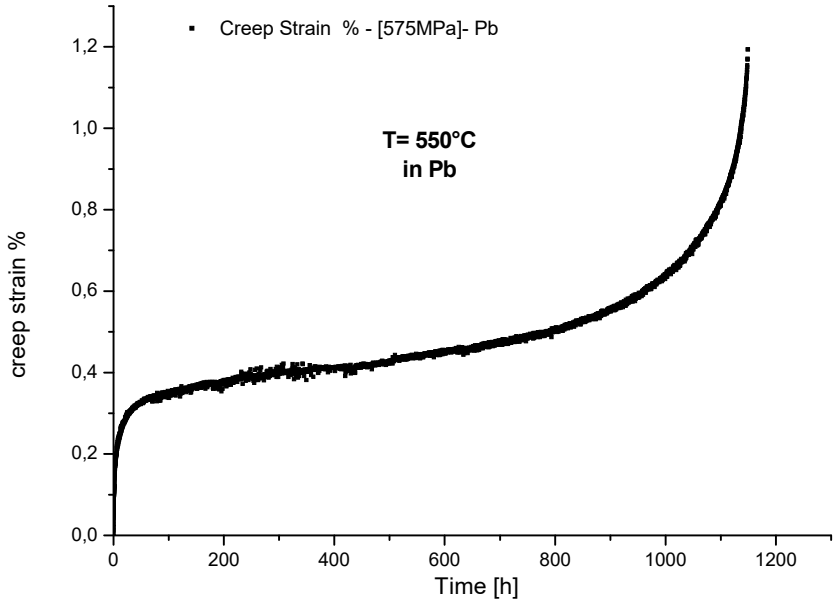

Figure 9: Creep curve in lead.

To highlight the lead effect, creep curve obtained from the test on specimen in air was compared with that obtained in lead. The comparison between creep curve in air and in lead at 560MPa is depicted in Fig. 11.
As expected, an increase in creep strain was observed, but it isn't really relevant, until the value of 800h: creep curves in lead and in air showed the same shape with a difference of creep strain percentage around 0.04% and it concerned only the primary creep; moreover, the strain rate is the same.

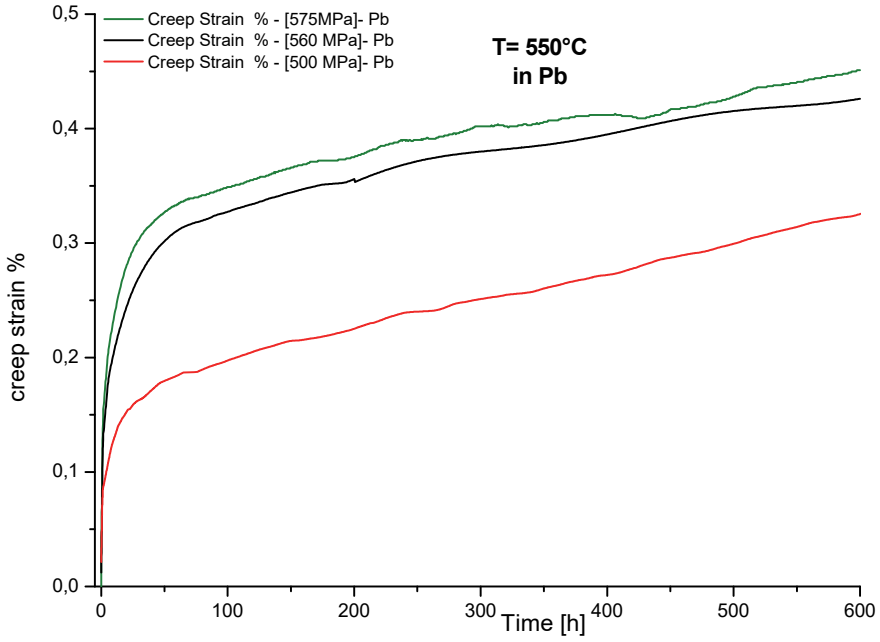

Figure 10: Creep curves of specimens tested in lead.

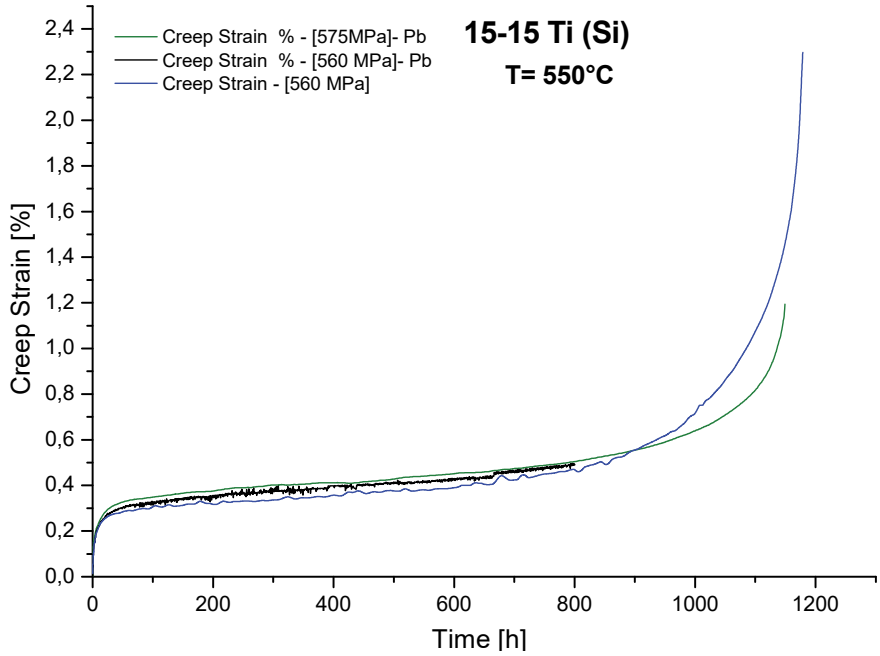

Figure 11: Comparison of 15-15Ti(Si) creep curves in air at 560MPa and in lead at 560 and 575Mpa.

Therefore, up to 800h, the behaviour of 15-15Ti(Si) in lead and in air at 560 MPa is almost similar. For these reasons the test in lead was stopped. An increase of steel deformation in lead took place, but it isn't relevant and it can be said that creep mechanisms seem to be predominant than lead corrosion. It could be ascribable to the stress value near yield stress[1] and it can be hypothesized that lead corrosion appears after a long time of steel/lead contact.
To better understand the effect of lead corrosion, it is necessary to discuss the test in lead at higher stress level, 575MPa, and its comparison with curves at 560MPa because it can provide important information on creep corrosion.

1 theoretical 620 MPa ≤ $R_{p0.002}$ ≤ 840 MPa, after 20% CW

Although they weren't obtained at the same stress level, creep curve at 575MPa in lead are plotted in Fig.11. It can be noticed that rupture time of specimen tested at 575MPa in lead is lower than that tested in air at 560MPa, as expected.
Up to 850h, creep strain of specimen in lead is higher than creep strain in air and this supports the hypothesis that lead corrosion appears after a long time of steel/lead contact. For time greater than 850h, it can be observed a trend inversion. It is due to LME, which produces a loss of ductility and competes with creep strain at higher stress and long time. Indeed, it can be noticed that the specimen tested at 575MPa in lead shows a lower percentage of final creep strain than specimen tested at 560MPa in air, although subjected to higher stress level, but it shows a lower time of rupture too; this means that it is less ductile than specimen tested in air and it is in accordance with LME effect.
It is important to underline that these tests in stagnant liquid lead were performed to verify the steel sensitivity to LME. The *Handbook on Lead-bismuth Eutectic Alloy and Lead Properties, Materials Compatibility, Thermalhydraulics and Technologies* [8] proposes the following definition of LME*: LME is the loss of ductility of a normally ductile metal or metallic alloy when stressed in contact with a liquid metal that can result in brittle fracture.* Typically the phenomenon is accompanied with a change from ductile to brittle fracture modes, intergranular or transgranular cleavage-like fracture modes.
According to this definition, the LME justifies the decrease of rupture time, the reduction of creep strain and then the loss of specimen ductility tested in lead.
The effect of lead is more evident at the lower stress (500MPa, Fig. 12). The comparison between curves in lead and air at 500 MPa can better explain this phenomenon: a relevant increment of deformation growths with the time in the whole curve, unlike tests at 560MPa. It means that lead influences the sscr, then the shape of creep curves. In addition, the lead presence anticipates the tertiary stage which occurs at about 700h, unlike test in air that remains in the secondary stage. All these effects are ascribable to LME.

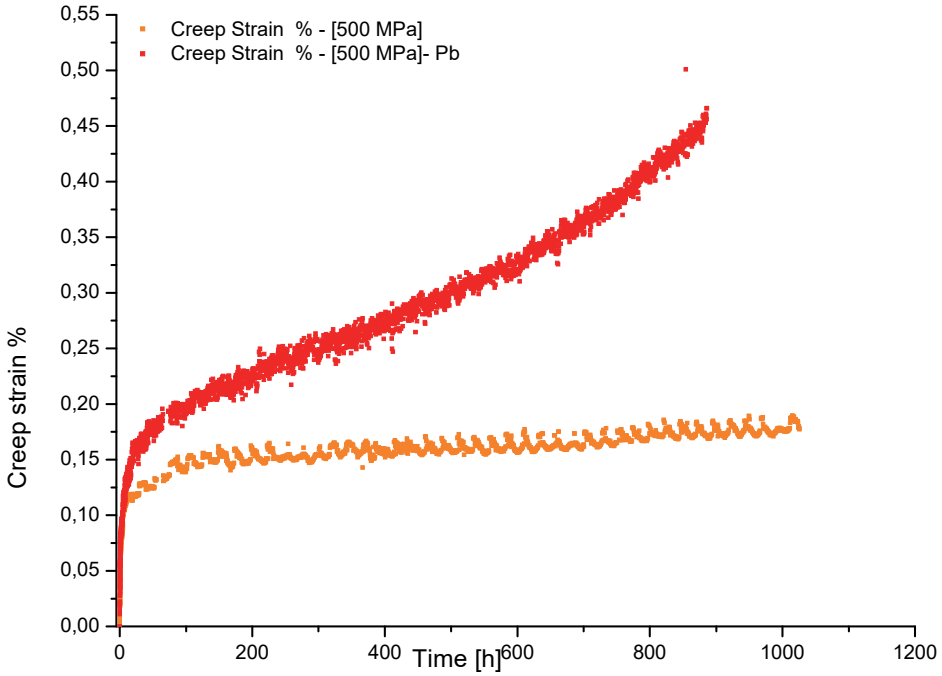

Figure 12: Comparison between creep curves 500MPa in air and in lead.

Then, the analysis on tests in lead can be summarized as follows:
- For high stresses (near yield stress) the presence of liquid lead does not significantly affect the deformation of the specimens and its deformation rate sscr. This means that the creep effect dominates the deformation in primary and secondary stages. The effect of Pb becomes prevalent only in the tertiary stage and it occurs with a reduction of the final time and final deformation percentage and then with a change in the rupture mode.
- For low stresses (significantly below the yield), the effect of Pb is more evident. It was noticed that lead influences sscr and increases the deformation, with the time. Then, LME tends to prevail on creep effect: the shape of curve changes, the sscr is higher than the test in air and the tertiary stage occurs at lower time.

Morphological and microstructural characterization

Steel specimens were observed by Optical and Scanning Electron Microscopy to characterize the raw materials and highlight the microstructure induced by 20% cold-working. Before the analysis, the steel samples were glyceregia etched for the examination of grains structure [9]. Glyceregia is indeed recommended for revealing the austenitic microstructure, as grain structure, and outlines carbides [10].

Slip produced by cold-working is shown in Fig. 13.

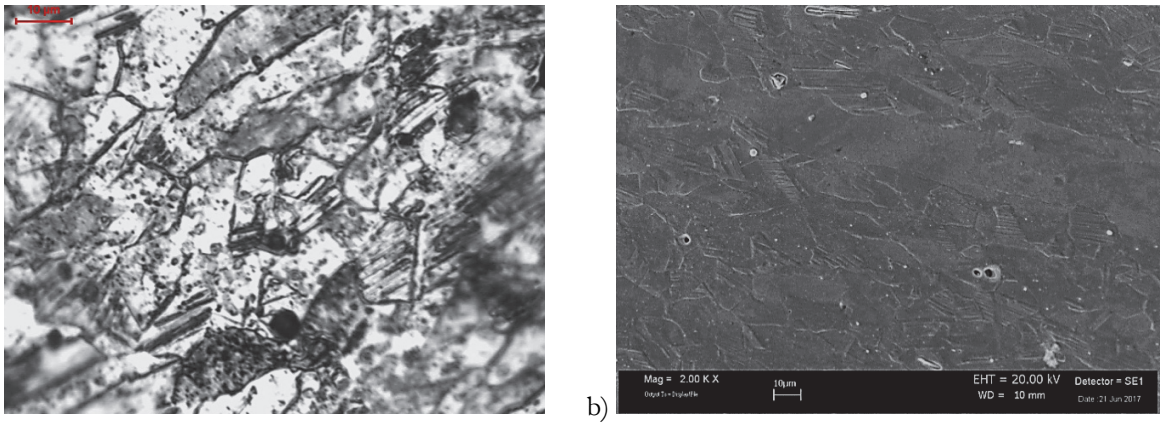

Figure 13: Glyceregia etched as received steel: a) Optical and b) SEM micrograph.

Moreover, the specimens were examined after rupture by scanning electron microscopy. Secondary electrons are used to obtain the fracture surface morphology.

Typical SEM images of fracture surfaces obtained from the creep specimens tested in air are shown in Fig. 14. Fig. 14-a concerns a low magnification and also includes an insert macroscopically displaying the specimen immediately after rupture. Both the specimen necking, identifying the ductile fracture, and the typical changes of fracture direction, characterizing the transgranular fracture, are pointed out. The fracture surface has a wrinkled appearance of mixed or ductile fracture. The micrographs of Figs. 14-b,c,d showed a combination of a cup-cone and transgranular fracture modes. The first one is characterized by its typical dimples, while the second one by the river pattern. The typical equiaxed dimples, characteristic of ductile fracture in tension, and then dominant cup-cone mode, are characteristic of surfaces close to central area of specimen (Fig. 14-b). Instead a transgranular fracture mode is dominant in the central part of specimen, where local facets of quasi-cleavage are noticed (Fig. 14-c). The other regions of the fracture surface are a combination of shear rupture (transgranular rupture) and cup-cone fracture (coalescence by shear of voids caused by plastic deformation). The transgranular rupture is incomplete, showing a mixed rupture mode, as in the case of external surface corresponding to the specimen necking. The deformation bands with the elongated dimples on the fracture surface are clearly displayed in Fig. 14-d. These considerations move to the conclusion that the specimen rupture mode is mixed, transgranular and cup-cone mode.

These observations are consistent with the expectations: the addition of Ti induces the precipitation of carbide particles and consequently the improvement of the high temperature mechanical properties, as creep strength, as reported by Zahra and Schroeder (1982) [11]. They studied creep properties of an austenitic steel with a chemical compositions similar to that of 15-15Ti(Si), finding that the fine TiC precipitates in Ti-stabilized austenitic stainless-steel cold-worked alloy form preferentially on the intergranular dislocations and they are more stable [11]. This justifies transgranular or ductile fracture.

Even for specimen tested in lead, morphological features of fracture surface was analyzed by Scanning Electron Microscopy (Fig. 15), but a chemical polishing was necessary to differentiate steel surface fracture from eventual lead residues and to reveal the fracture mode. The Fig. 15-a also includes an insert macroscopically displaying the specimen immediately after rupture. The loss of steel ductility and the typical brittle fracture are evident from the brilliant and polished fracture surface, along 45°, with negligible plastic deformation.

It can be observed that the fracture is brittle, as showing by the typical intergranular fracture, where the decohesion occurring along a weakened grain boundary is evident (Fig. 15-b). Grains are clearly observed in their three-dimensional structure, within a polished fracture surface with no wrinkled appearance, unlike ductile materials (Fig. 14).

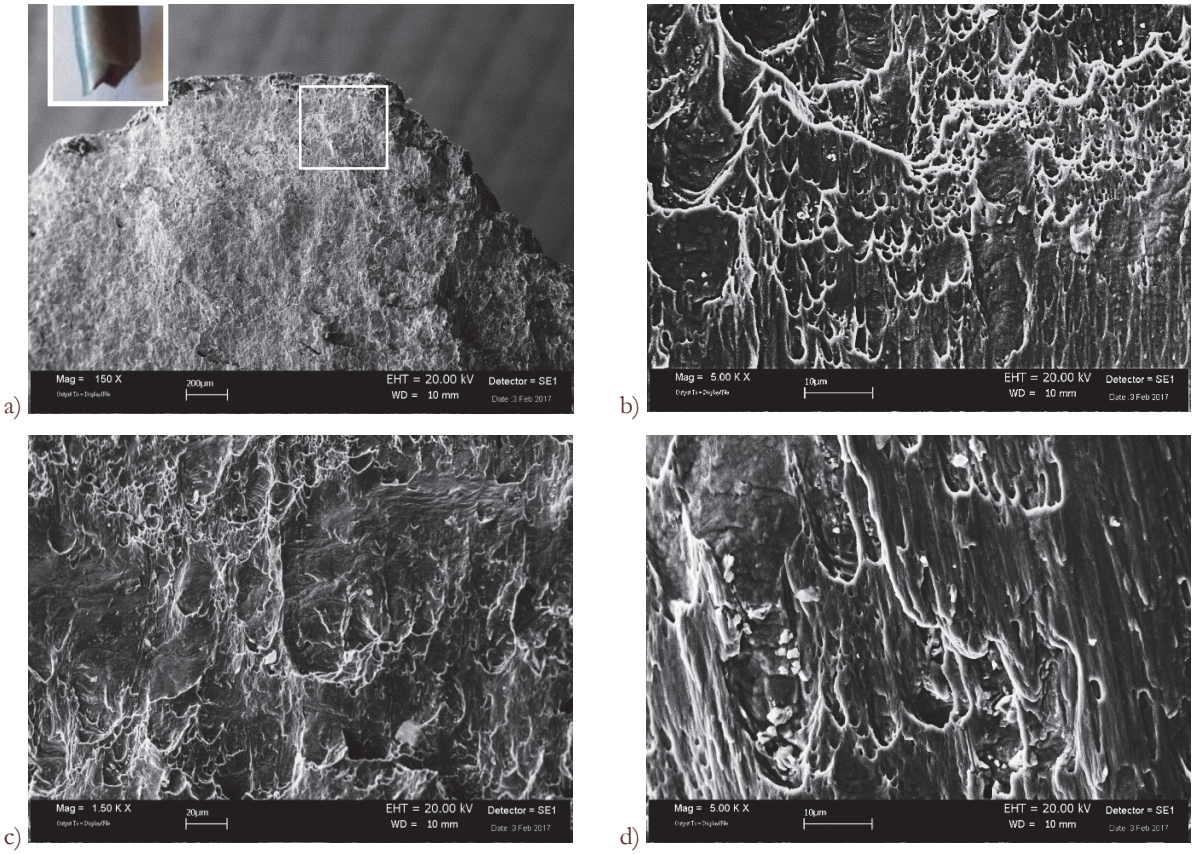

Figure 14: SEM micrographs: a) fracture surface at low magnification; b) portion of surface showing a dominant ductile fracture mode; c) portion of surface showing both transgranular and ductile fraction; d) deformation bands: elongated dimples on fracture surface.

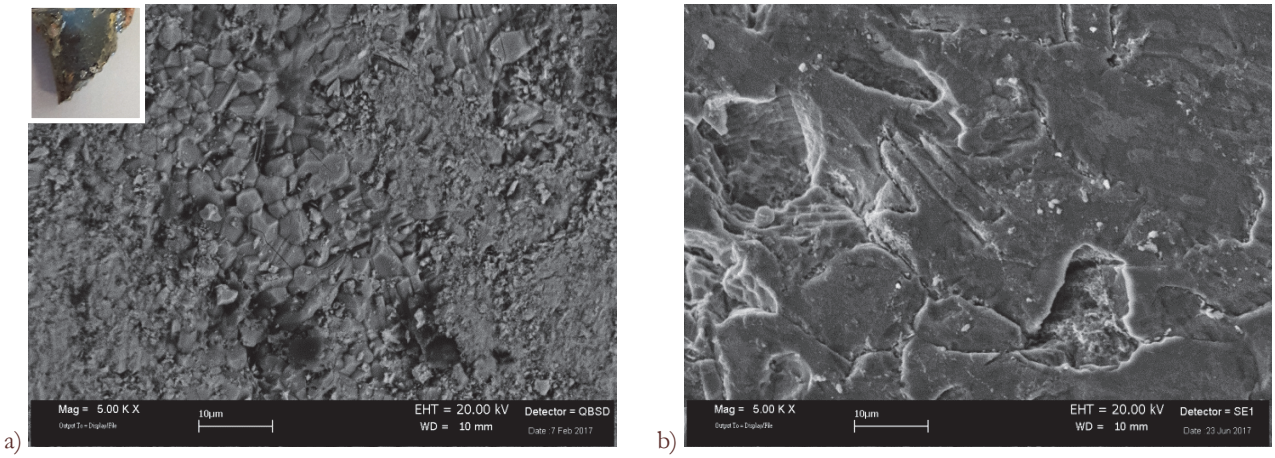

Figure 15: SEM micrographs after Pb creep: fracture surface a) before and b) after chemical polishing.

The comparison between the specimen tested in air and in lead revealed a different fracture mode: mixed cup-cone/transgranular for creep test in air, while intergranular for creep test in lead. This difference is ascribable to the effect of lead embrittlement: the transition from mixed fracture mode, ductile/transgranular, which takes place in air, to fully brittle/intergranular mode, in lead, is consistent with the definition of LME (stated in paragraph 3.2) and with the creep phenomena in liquid metal, as described in other scientific works.
According to Hough and Rolls (1971)[12], phenomena associated with creep rupture in liquid metal can include:

- cracking induced by the adsorption of liquid metal atoms
- accelerated failure due to the penetration of the liquid metal along the grain boundary of the solid
- stress - aided dissolution of metal from a crack tip

These considerations can justify the intergranular fracture mode: intergranular fracture usually occurs when the phase in the grain boundary is weak and brittle and this is probably due to the penetration of the liquid metal along the grain boundary of the steel which caused the embrittlement of phases and then the accelerated failure.
It means that lead changes both mode and type of fracture: from mixed ductile/brittle to total brittle and, referring to brittle mode, from transgranular to intergranular type. That is the effect of liquid metal embrittlement [13].

CONCLUSIONS

The creep and corrosive behavior of the 15-15Ti(Si), for the nuclear systems using heavy liquid metals, has been addressed. For this purpose, the steel has been studied in a stress range of 300-575MPa at 550°C, in air and in hostile environment. From tests performed in air, the characteristic creep curve strain-time was obtained. The Norton's law parameters n and A were calculated and it was found that the dislocation creep mechanism is the main mechanism for the 15-15Ti(Si) creep deformation. The creep curve sscr-stress (log–log plot) was plotted based on Norton's law, on experimental data and on the calculated values n and A. This curves is an important results because simulates the creep behaviour of 15-15Ti(Si) in air at all stress values.
SEM micrographs showed that the specimen fracture mode in air was mixed, transgranular and cup-cone.
Tests in lead were also performed and the main results can be summarized as follows:
- For high stresses, the creep effect dominates the deformation in primary and secondary stages, while the effect of Pb becomes prevalent in the tertiary stage
- For low stresses, the effect of Pb is more evident and LME tends to prevail on creep effect.

The specimen rupture mode in lead is brittle, as confirmed by SEM micrographs that highlights the typical intergranular fracture. Moreover, the differences between mixed fracture mode, ductile-brittle/transgranular, occurring in air and fully brittle/intergranular mode, in lead were shown.
It means that liquid metal embrittlement occurs: lead changes both the mode and type of fracture, from mixed ductile/brittle to total brittle and, referring to brittle mode, from transgranular to intergranular type.
Since only few data on 15-15Ti(Si) characterization can be found in the literature, the obtained results provide useful information for this austenitic steel applications in extreme conditions, such as nuclear field.

ACKNOWLEDGEMENT

The authors are grateful to Dr. Selene Grilli for her careful revision of the manuscript. We also acknowledge the C.R. ENEA Brasimone for financial support and providing the samples to be tested.

REFERENCES

[1] Latha, S., Mathewa, M.D., Parameswaran, P., Bhanu Sankara Rao, K., Mannan, S.L., Thermal creep properties of alloy D9 stainless steel and 316 stainless steel fuel clad tubes, International Journal of Pressure Vessels and Piping, 85 (2008), 866–870 Elsevier
[2] Gilbon, D., Séran, T.L., Maillard, A., Touron Rivera, H.C., Lorant, H., Permet, J., Rabouille, O. Swelling microstructure of neutron irradiated Ti-stabilized austenitic steels, International conference on materials for nuclear reactor core applications, Bristol (UK), (1987) 27-29.
[3] IAEA, International Atomic Energy Agency. Nuclear Energy Series Technical Reports Structural Materials for Liquid Metal Cooled Fast Reactor Fuel Assemblies — Operational Behaviour No. NF.T.4.3 Guides- Printed by the IAEA in Austria (2012).
[4] Vaidya Gkss, W.V., Radiation-induced recrystallization, its cause and consequences in heavy-ion irradiated 20% cold-drawn steels of Type 1.4970, Journal of Nuclear Materials 113, North.Holland Publishing Company, (1983) 149-162.

[5] Wilson, F. G., Pickering, F. B., A study of zone formation in an austenitic steel containing 4% Titanium. Acta Metallurgica, 16 (1968) 115-131
[6] Daenner, W., A comparison of AISI type 316 and German type DIN 1.4970 stainless steel with regard to the first-wall lifetime. Journal of Nuclear Material. North. Holland Publishing Company, 103 & 104 (1981) 121-126
[7] Caro, M., Woloshun, K., Rubio, F. and Maloy, S., Materials Selection for the Lead-Bismuth Corrosion and Erosion Tests in DELTA Loop Los Alamos National Laboratory, (2013).
[8] NEA Expert Group on Heavy Liquid Metal Technologies. Handbook on Lead-bismuth Eutectic Alloy and Lead Properties, Materials Compatibility, Thermalhydraulics and Technologies- Nuclear Energy Agency Organisation For Economic Co-Operation And Development, (2015) 487-570.
[9] Nelson, D. E., Baeslack, W. A., Characterization of the Weld Structure in a Duplex Stainless Steel Using Color Metallography Metallography, 18 (1985) 215-225.
[10] Radzikowska, J.M., Metallography and Microstructures of Cast Iron, Metallography and Microstructures, ASM Handbook, ASM International, 9 (2004) 565–587.
[11] Abou Zahra, D-A., Schroeder, H. The dependence of the creep properties of DIN 1.4970 austenitic stainless steel at 973 K on different thermomechanical pre-treatments, Journal of Nuclear Materials, North.Holland Publishing Company, 107 (1982) 97-103.
[12] Hough, R.R., Rolls, R., Creep fracture phenomena in iron embrittled by liquid copper, Journal of Material Science, 6 (1971) 1493-1498.
[13] Strafella, A., Coglitore, A., Salernitano, E., Creep behaviour of 15-15Ti(Si) austenitic steel in air and in liquid lead at 550°C, Procedia Structural Integrity, 3 (2017) 484-497.